Supplementary Information

Supplementary Results

RNA binding of Loqs dsRBDs

Since the two N-terminal dsRBDs of Loquacious also participate in the biogenesis of miRNAs in the context of the Dcr-1/Loqs-PB complex, we also studied the "diced" miRNA/miRNA*-duplex and the pre-miRNA forms of *bantam*. Finally, we engineered a short, 14 bp duplex with a blunt end on one side. To perform fluorescence anisotropy measurements, a fluorophor (FITC) was attached to the model substrates at the first nucleotide of the 2 nt 3'-end single-stranded overhang (i.e. directly adjacent to the double-stranded part). We determined comparable binding constants with model substrates of siRNA and miRNA/miRNA* duplexes based on the *Drosophila* miR-8 sequence, indicating that independent binding of the two domains was not specific for the *bantam* based model substrates (**Supplementary Figure 3D**). Full-length Loqs-PD displayed a moderate preference for binding of siRNAs and 35 nt dsRNA compared with the pre-miRNA and miRNA/miRNA* substrates (50 and 62 nM vs., 118 and 100 nM, Wilcox Rank sum test, $p=0.029$ and 0.028).

For our binding assays (fluorescence anisotropy) we noticed that Hill coefficients greater than one were required for curve fitting (**Table 4**). This was not a technical artifact specific to our anisotropy-based measurements, since binding assays using electrophoretic mobility shift assays (EMSA) resulted in a comparable binding curve (**Supplementary Figure 3C**).

Biophysical characterization of Loqs dsRBDs and linker mutants

The molecular weights determined by SEC for single domains (dsRBD1, residues 129-211, 9.1 kDa and dsRBD2, residues 245-322, 9.2 kDa) and SEC-SLS Loqs-PD$_{\Delta NC}$ (21.0 kDa) demonstrate that these proteins are monomeric (data not shown). In contrast, Loqs-PD$_{\Delta N}$ was observed as a dimer as determined by SAXS (**Supplementary Table 2**).

The protein linker mutants exhibited only minor chemical shift changes with the exception of the residues flanking the deleted regions (**Supplementary Figure 7B**) in our NMR spectra, confirming that the domains do not contact each other. Loqs-PD$_{\Delta NC\Delta 41}$ however, showed smaller CSPs and some peaks shift backwards towards the chemical shift of the free protein. This indicates that by deleting almost the entire linker the mobility and uncoupling of the dsRBDs is impaired.

We observed that the chemical shift perturbations upon RNA binding were only marginally affected by shortening of the linker (**Supplementary Figure 7C)**, unless almost the entire linker (Δ209-249 = Loqs-PD $_{\Delta 41}$) was deleted, in which case all signals in the NMR spectrum experienced severe line-broadening (data not shown). This might indicate the formation of intermolecularly connected protein-RNA networks with high molecular weight. In any case, the data show that a wild type linker length is not essential for RNA binding.

Supplementary Methods

Genome editing and deep sequencing of small RNAs in S2 cells

S2 cells were transfected with pRB14 and PCR products for sgRNA expression as previously described (1). Single-cell clones were then established and screened via PCR amplification and T7 endonuclease reactions for the presence of mutations. Homozygous mutant clones were identified by lack of detectable protein in Western blots and then confirmed by sequencing. The oligonucleotides used for sgRNA expression were 5'-taatacgactcactataGCGGCACTATAATAACCTTGTgttttagagcta-3' for Loqs and 5'-taatacgactcactataGGAGATAGAGGCCCTTGGAAAgttttagagcta-3' for R2D2. The antibodies against Loqs and R2D2 were kind gifts of Dr. Mikiko Siomi. Small RNA library preparation was performed as described (2).

First, we checked whether the abundance of miRNA-matching and transposable-element matching siRNA reads are differentially affected by the genotype. To this end, we log-transformed the raw read counts (to avoid predominance of highly abundant species) from all untreated sequencing runs and then plotted these values for the r2d2-mutant vs. the loqs-mutant cell lines. A systematically lower read count in e.g. the loqs mutant cell line for one of the small RNA species will result in a change of the slope of a trendline through all corresponding datapoints, while a difference in sequencing depth will affect the axis intercept. The difference in the slope of miRNA vs. endo-siRNA reads is a measure for one of the small RNA species being more sensitive to factor deletion. We did not see a strong and systematic difference in miRNA vs. endo-siRNA abundance (endo-siRNAs 1.1 +/- 0.02 fold more strongly reduced than miRNAs upon deletion of loqs). It has previously been noted that, while loqs mutants do show an increase in pre-miRNA levels, the mature miRNAs on average showed a rather mild reduction in the soma, e.g. (3). Individual species, such as miR-305 did show an appreciable dependence on Loqs-PB and we could detect this effect in our sequencing data for the loqs mutant (raw read counts):

	1_19_3 (r2d2)	3_19_35 (loqs)	*ratio l/r*	2_7_13 (r2d2)	3_7_25 (loqs)	*ratio l/r*
miR-305-5p	21502	2239	*0,104*	8293	1159	*0,140*
miR-277-3p (control)	51369	41590	***0,810***	14575	11451	***0,786***

However, the reduction in miRNA levels on average largely corresponds to the effects on siRNA levels. Finally, we verified that there is no systematic shift in miRNA positions between the r2d2 and loqs mutant datapoints in the comparative diagrams (Suppl. Fig. 2D and E).

Based on this, we decided to normalize all datasets to the number of miRNA-matching reads since these are predominantly beta-elimination sensitive in all genotypes. This allowed us to arrange the two-dimensional data for r2d2 vs. loqs mutant cells in a single plot for direct comparison. These can be found in Fig. 1 A and in supplementary Fig. 2 A-C. Consistently, the endo-siRNA datapoints showed a greater extent of beta-elimination sensitivity in the loqs mutants vs. the r2d2 mutants. For a quantitative analysis, we log-transformed the data to mitigate the influence of highly abundant species and then calculated trendlines by linear regression. In this case, the slope of the trendline was unaffected by genotype while the axis intercept was systematically lower for the loqs mutant clones. After back-transformation, we find that the transposon-targeting endo-siRNAs were 3.5 +- 0.9 fold more sensitive to beta-elimination in the loqs mutant than in the r2d2 mutant cells. This effect was consistent in all three replicates (Supplementary Fig. 2 A-C, $p < 0.03$, paired t-test).

Protein expression, purification and NMR sample preparation

Constructs with varying linker lengths were expressed in the same vector and purified as follows. The soluble fraction of the target protein decreased with decreasing linker length. Protein expression was induced with 0.5 mM Isopropyl beta-D-1-thiogalactopyranoside (IPTG) at an OD_{600} ~0.8. After expression at 20°C for ~ 16 hours the cells were harvested by centrifugation, resuspended in lysis buffer (50 mM Tris pH 8.0, 1 M NaCl, 10 mM imidazole, 5 mM β-Mercaptoethanol), incubated with lysozyme, DNase and EDTA-free protease inhibitor on ice and sonicated. After lysis the supernatant was applied to a Ni-NTA column and washed with half a column volume of 1 M LiCl (50 mM Tris pH 7.2, 10 mM Imidazole, 5 mM β-Mercaptoethanol) buffer followed by three column volumes of the same buffer with LiCl replaced by 1 M NaCl. Afterwards the protein was eluted with 400 mM Imidazole (50 mM Tris pH 7.5, 200 mM NaCl, 5 mM β-Mercaptoethanol). The His-tag was cleaved by 0.1 mg TEV protease/mg protein in presence of 2

mM DTT at 4°C for 20 hours and afterwards separated from the protein by another Ni-NTA chromatography step. For further purification the eluate was applied to a Superdex 75 column using a 500 mM NaCl, 0.1 mM EDTA and 5 mM DTT buffer with either 20 mM HEPES (pH 7.2) or 20 mM sodium phosphate (pH 6.5). These buffers were used to concentrate samples to 200 µM using a centricon device. For structure determination phosphate buffer was used whereas titration experiments were performed in HEPES buffer (20 mM HEPES pH 7.2, 500 mM NaCl, 0.1 mM EDTA, 10 mM DTT). Only the 12-mer RNA was titrated in phosphate buffer at pH 7.2.

For NMR experiments single-strands of the *bam*-siRNA (5'-UCAGCUUUCAAAAUGAUCUCACU-3', 5'-UGAGAUCAUUUUGAAAGCUGAUU-3') were purchased from IBA GmbH (Göttingen, Germany) and dissolved in annealing buffer (20 mM sodium phosphate pH 6.5, 50 mM NaCl, 2 mM DTT, 0.1 mM EDTA), mixed in equimolar amounts and annealed using a temperature gradient from 95°C to 4°C in a thermocycler. Successful annealing was verified by imino NOESY spectra recorded at 278 or 298 K (data not shown).

NMR spectroscopy

For NMR chemical shift assignments different isotope-labelling schemes were prepared. One RNA strand was uniformly ^{15}N, ^{13}C or a nucleotide (A or G)-selective isotope labelled and annealed with an unlabeled pairing strand. The labelled nucleotides were purchased from Silantes GmbH (München, Germany).

RNA chemical shift assignments were based on ^{1}H NMR spectra including imino ^{1}H NOESY, NOESY and TOCSY in H_2O and D_2O buffer, $^{1}H,^{15}N$ SOFAST-HMQC, $^{1}H,^{15}N$ HSQC and $^{1}H,^{13}C$ HSQC experiments (4) with samples at 300-400 µM concentration. For comparison of free and complexed RNA imino NOESY, ^{1}H TOCSY, $^{1}H,^{15}N$ HSQC and $^{1}H,^{13}C$ HSQC spectra were used with a protein:RNA ratio for the complex of 1.3:1.0 at an RNA concentration of 80-150 µM. All spectra were recorded at 298K except for the imino NOESYs of the purchased *bam*-siRNA (278K).

For PRE experiments the *bam*-siRNA was chemically synthesized and a TEMPO-radical was attached to both 5' ends as described (5). Each spin-labelled strand was annealed with the respective pairing but unlabeled strand for NMR spectroscopy as described above. Successful incorporation of the spin label was proven by mass spectrometry, HPLC and NMR spectroscopy (data not shown). Prior to the PRE experiments incorporation and integrity of the TEMPO spin label were tested by 1D NMR spectroscopy of the paramagnetic and diamagnetic (upon reduction with ascorbic acid) free dsRNA. To measure intermolecular PREs between the RNA and protein, the annealed dsRNA was mixed with ^{15}N labelled

Loqs-PD$_{\Delta NC}$ at a protein:RNA ratio of 1:1.5 in HEPES buffer (s. above). The spin label was reduced by addition of pH adjusted ascorbic acid in a 4 to 5-fold excess. For both paramagnetic and diamagnetic states HSQCs with high numbers of scans were recorded. The PRE effect was determined by calculating the intensity ratio of the para- and diamagnetic spectra. We used 1D spectra of the complex to confirm that the spin label is intact and only reduced upon addition of ascorbic acid.

Structure calculations

Structure calculations using ROSETTA were based on NMR chemical shifts and NOE data. The structures of dsRBD1 and dsRBD2 were calculated using CS-Rosetta (6) and CS-RASREC-Rosetta (7), respectively. Backbone and side-chain chemical shifts and unassigned NOE peak lists were combined and included with CS-RASREC-ROSETTA as described (7).

Static Light Scattering

SLS measurements on Loqs-PD$_{\Delta NC}$, *bam*-siRNA and the complex were performed by connecting a Viscotek TDA 305 triple-array detector to an Äkta Purifier equipped with an analytical size-exclusion column at 4°. Samples in 250 mM NaCl 20mM Tris pH 6.5 were passed through a GE Superdex200 10/300 column at a flow rate of 0.5 ml/min. The sample concentrations used were 3.8 mg/ml for Loqs-PD$_{\Delta NC}$, 1800 ng/µl for dsRNA and 4.1 mg/ml protein at a 3:1 ratio for the complex. The molecular masses of the samples were calculated from the experimentally determined refractive index and right-angle light-scattering signals using the Omnisec software package (Malvern Instruments). The SLS detector was calibrated with a bovine serum albumin solution (4 mg/ml), taking 66.4 kDa as the molecular mass of the bovine serum albumin monomer and assuming a dn/dc value of 0.185 ml/g for protein, 0.165 for RNA and 0.177 for a 1:1 complex.

Small-angle X-Ray scattering

SAXS measurements were performed on a Rigaku BIOSAXS1000 instrument with a HF007 microfocus generator equipped with a Cu-target at 40kV and 30mA. A Pilatus 100k detector was used for image collection. Transmissions were measured with a photodiode beamstop, and a silver-behenate sample was used for q-calibration. Measurements were made in multiple 900 sec frames checked for beam damage and averaged. Circular averaging and background subtraction was done with the Rigaku SAXSLab software. Distance distribution functions *P*(r) were calculated with GNOM, rigid body modeling was performed using CORAL, both within the ATSAS package v 2.6.0-1(8). Molecular weights were calculated from POROD volumes as described.

RNA sample preparation

For binding experiments, *bantam* 23 nt sense (5'-UGAGAUCAUUUUGAAAGCUGAU*U-3') and siRNA antisense (5'-UCAGCUUUCAAAAUGAUCUCACU-3') or miRNA antisense (5'-UCGGUUUUCGAUUUGGUUUGACU-3') were annealed by heating to 95°C followed by slow cooling to RT to create double stranded *bam*-siRNA or miRNA duplexes with 2nt 3' overhangs. The asterisk in the sequence follows the position of the fluorescently labeled (FITC) nucleotide. The oligonucleotide *bantam* 35 nt sense (5'-GAUUCAUACAAGUGAGAUCAUUUUGAAAGCUGAU*U-3') was annealed with *bantam* 35 nt antisense (5'-UCAGCUUUCAAAAUGAUCUCACUUGUAUGAAUCAA-3') to create a 33 nt dsRNA precursor with 2nt 3' overhangs. For the miRNA precursor, *bantam* 23 nt sense was ligated to 5'-phosphorylated *bantam* stemloop (5'-UCGGUUUUCGAUUUGGUUUGACUGUUUUUCAUACAAG-3') and the ligation product was gel purified. The 14 nt blunt end duplex resulted from annealing two shortened *bantam* 23 nt sense and siRNA antisense oligos (5'-UGAGAUCAUUUUGA-3' and 5'-U*CAAAAUGAUCUCAUU-3').

Thiouridine containing oligos were annealed with *bantam* 23 nt sense (5'-UGAGAUCAUUUUGAAAGCUGAUU-3') or siRNA antisense to obtain siRNA duplexes with one 4-thio-uridine each. Nicked siRNA duplexes were created by annealing a split *bantam* 23 nt sense (5'-UGAGAUCAUUUU-3' and 5'-GAAAGCUGAUU-3') or siRNA antisense (5'-UCAGCUUUCAA-3' and 5'-AAUGAUCUCACU-3') to their thiouridine or FITC containing partner strands. RNA oligos with the depicted modifications were ordered from Thermo Fisher scientific. All oligonucleotides were 5'-phosphorylated with polynucleotide kinase and either radioactive or non-radioactive ATP, followed by removal of the unincorporated nucleotide.

To study the impact of protein binding on the RNA structure, both *bam*-siRNA strands were produced by *in vitro* transcription as single strands according to Milligan et al. (1987). At both ends bases were changed to GG at the 5' terminus for higher transcription efficiency. The two template strands including a reverse complementary T7 polymerase binding site and the T7 top strand were ordered from Eurofins Genomics GMBH, Ebersberg. After optimization of $MgCl_2$ concentration, transcriptions were performed in preparative batches of 5 or 10 ml. For a 5 ml transcription first annealing of both T7 top strand (TAATACGACTCACTATAG) and the respective template strand (5'-AAGGAGATCATTTTGAAAGCTCCTATAGTGAGTCGTATTA-3', 5'-AAGGAGCTTTCAAAATGATCTCCTATAGTGAGTCGTATTA-3') in presence of $MgCl_2$ (480 nM T7 top strand, 400 nM template strand, 40 mM $MgCl_2$) was made in a thermocycler by a temperature gradient from 90°C to 10°C. Afterwards the strands were added to the reaction mixture (1xTRX-buffer,

40mM Mg Cl_2, 500mg/ml PEG8000, ATP/CTP/GTP/UTP 4mM each, 0.5 mgl/ml T7 RNA polymerase) and incubated at 37°C for 5 hours. By centrifugation for 10 min at 14000g the precipitate could be removed and the supernatant was ethanol precipitated (0.1x volume 3M NaAcO pH 5.5, 3.5x volume 100% cooled ethanol) at -20°C overnight. The RNA was pelleted by centrifugation,air dried to remove remaining ethanol and afterwards resuspended in 2-3 ml loading buffer (0.25% Bromphenol Blue, 30% glycerol, 1xTBE buffer). For purification the RNA was loaded onto a 8M Urea 20% acrylamide gel (0.5x TBE as running buffer) and the gel was run for 15 hours at constant 30W. The target RNA band was identified under UV light and cut out. To recover the RNA from the gel, electroelution in 0.5x TBE was used. The RNA was eluted at 200V and progress was monitored by determining the RNA concentration at the Nanodrop. Elution was essentially complete after 8 hours. The RNA was dialyzed against 1M NaCl and afterwards twice against ddH_2O. At last the RNA was lyophilized and stored at -20°C. For NMR experiments the RNA was dissolved in either HEPES buffer (see above) for titrations or 50 mM NaCl, 20 mM sodium phosphate pH 6.5 for both RNA assignment experiments as well as complex spectra with Loqs-PD. As described previously the strands were annealed via a temperature gradient.

Supplementary Tables

Supplementary Table 1: Dali alignments for dsRBD1 and dsRBD2

dsRBD1

No	Chain	Z	rmsd	lali	nres	%id	PDB Description
1	1rc7-A	7.8	2.2	60	220	33	Ribonuclease III
2	3llh-B	7.7	2.3	59	66	42	RISC-Loading Complex Subunit TARBP2
3	3adl-A	7.6	2.0	59	76	27	RISC-Loading Complex Subunit TARBP2
4	1di2-A	7.6	2.1	59	69	29	Double Stranded RNA Binding Protein A
5	2nuf-A	7.6	2.2	61	219	33	28-mer
6	1yz9-A	7.6	2.2	60	220	33	Ribonuclease III
7	2nuf-B	7.5	2.3	61	219	33	28-mer
8	2nug-B	7.5	2.2	61	218	34	5’-R(P*AP*AP*GP*GP*UP*CP*AP*UP*UP*CP*G)-3’
9	1yz9-B	7.5	2.5	61	218	33	Ribonuclease III
10	1yyk-A	7.4	2.2	60	221	33	Ribonuclease III

dsRBD2

No	Chain	Z	rmsd	lali	nres	%id	PDB Description
1	1di2-A	11.1	1.6	66	69	41	Double Stranded RNA Binding Protein A
2	3adl-A	10.6	1.6	66	76	41	RISC-Loading Complex Subunit TARBP2
3	1rc7-A	10.1	1.9	66	220	35	Ribonuclease III
4	2nug-B	10.1	2.0	66	218	35	5’-R(P*AP*AP*GP*GP*UP*CP*AP*UP*UP*CP*G)-
5	1yyk-A	10.0	1.8	66	221	35	Ribonuclease III
6	2nue-B	10.0	1.7	66	220	35	46-mer
7	1yyw-	10.0	1.6	66	219	35	Ribonuclease III
8	1yyw-	10.0	1.7	66	219	35	Ribonuclease III
9	2nuf-A	9.9	2.0	66	219	35	28-mer
10	1yz9-A	9.9	1.9	66	220	35	Ribonuclease III

Supplementary Table 2: SAXS data of Loqs-PD$_{\Delta NC}$ and Loqs-PD$_{\Delta N}$ concentration series

Sample	R_g [Å]	D^{max} [Å]	Porod [Å^3]	MW [kDa]	theoretical MW [kDa]
Loqs-PD$_{\Delta NC}$ 1.9 mg/ml	30.05 ± 0.80	104.9	29324.9	23.8	21.0
Loqs-PD$_{\Delta NC}$ 3.6 mg/ml	32.73 ± 0.86	104.6	21501.0	17.4	21.0
Loqs-PD$_{\Delta NC}$ 4.2 mg/ml	32.18 ± 0.77	102.2	22139.7	17.9	21.0
Loqs-PD$_{\Delta NC}$ 4.9 mg/ml	30.65 ± 1.05	104.6	23269.3	18.8	21.0
Loqs-PD$_{\Delta N}$ 1.5 mg/ml	35.00 ± 1.00	167.2	52269.1	42.3	25.1
Loqs-PD$_{\Delta N}$ 3.4 mg/ml	36.60 ± 0.60	169.1	64776.1	52.5	25.1
Loqs-PD$_{\Delta N}$ 4.1 mg/ml	36.96 ± 1.96	177.1	63507.2	51.4	25.1
Loqs-PD$_{\Delta N}$ 4.6 mg/ml	38.30 ± 1.90	177.6	65321.1	52.9	25.1

Supplementary references

1. Bottcher, R., Hollmann, M., Merk, K., Nitschko, V., Obermaier, C., Philippou-Massier, J., Wieland, I., Gaul, U. and Forstemann, K. (2014) Efficient chromosomal gene modification with CRISPR/cas9 and PCR-based homologous recombination donors in cultured Drosophila cells. *Nucleic Acids Res*, **42**, e89.
2. Elmer, K., Helfer, S., Mirkovic-Hosle, M. and Forstemann, K. (2014) Analysis of endo-siRNAs in Drosophila. *Methods Mol Biol*, **1173**, 33-49.
3. Fukunaga, R., Han, B.W., Hung, J.H., Xu, J., Weng, Z. and Zamore, P.D. (2012) Dicer partner proteins tune the length of mature miRNAs in flies and mammals. *Cell*, **151**, 533-546.
4. Sattler, M., Schleucher, J. and Griesinger, C. (1999) Heteronuclear multidimensional NMR experiments for the structure determination of proteins in solution employing pulsed field gradients. *Prog. NMR Spectrosc.*, **34**, 93-158.
5. Wunderlich, C.H., Huber, R.G., Spitzer, R., Liedl, K.R., Kloiber, K. and Kreutz, C. (2013) A novel paramagnetic relaxation enhancement tag for nucleic acids: a tool to study structure and dynamics of RNA. *ACS Chem Biol*, **8**, 2697-2706.
6. Shen, Y., Lange, O., Delaglio, F., Rossi, P., Aramini, J.M., Liu, G., Eletsky, A., Wu, Y., Singarapu, K.K., Lemak, A. *et al.* (2008) Consistent blind protein structure generation from NMR chemical shift data. *Proc Natl Acad Sci U S A*, **105**, 4685-4690.
7. Lange, O.F. (2014) Automatic NOESY assignment in CS-RASREC-Rosetta. *J Biomol NMR*, **59**, 147-159.
8. Petoukhov, M.V., Franke, D., Shkumatov, A.V., Tria, G., Kikhney, A.G., Gajda, M., Gorba, C., Mertens, H.D., Konarev, P.V. and Svergun, D.I. (2012) New developments in the ATSAS program package for small-angle scattering data analysis. *Journal of applied crystallography*, **45**, 342-350.
9. Forstemann, K., Horwich, M.D., Wee, L., Tomari, Y. and Zamore, P.D. (2007) Drosophila microRNAs Are Sorted into Functionally Distinct Argonaute Complexes after Production by Dicer-1. *Cell*, **130**, 287-297.

Supplementary Figures

Supplementary Figure 1: Loading of Ago2 by RLC and alternative RLC

A) Schematic overview of the Loqs alternative isoforms, Loqs-PD interacts with Dcr-2. After the dicing of dsRNA into siRNAs, two distinct RISC loading complexes exist in S2-cells: conventional RLC composed of Dcr-2 + R2D2 and alternative RLC composed of Dcr-2 + Loqs-PD.
B) Characterization of the mutant cell lines generated via *cas9*-CRISPR mediated genome editing. A series of single-cell clones was tested via western blotting using monoclonal antibodies (a kind gift of Dr. Mikiko Siomi) against Loqs (upper panel) or R2D2 (middle panel). The membranes were stained for total protein after the experiment as a loading control (bottom panel). The clones used for the experiments shown in Fig. 1 of the main text are 1-19-3 (no R2D2) and 3-19-35 (no Loqs).
C) Drosophila miR-277 is diced by Dcr-1/Loqs-PB but then a substantial fraction is loaded into Ago2 via Dcr-2/R2D2 RLC. This fraction can be selectively interrogated with a perfect match miR-277 GFP reporter (9). We demonstrate that for S2-cells, both forms of RLC are active in parallel using reporter assays that detect the activity of RLC-loaded miR-277 (R2D2-dependent) and of aRLC loaded endo-siRNAs (Loqs-dependent, see arrows).

Supplementary Figure 2: Further deep sequencing data analysis

A-C) Trendline analysis of the three independent biological replicates of our siRNA-loading analysis. In all cases, the transposon-targeting endo-siRNAs were more sensitive to β-elimination in the loqs mutant clones (3-19-35 and 3-7-25) than in the r2d2 mutant ones (1-19-3 and 2-7-13). The slopes and axis intercepts derived from the trendline analysis are indicated on the top right.
D) Analysis of individual miRNA positions in the *r2d2* and *loqs* mutant clones; the datapoints are identival to the miRNAs in A and B, for simplicity the endo-siRNA data was removed. For a selected set of miRNAs, we annotated the exact position of both, the 5'- and the 3'-product of the pre-miRNA hairpin. Changes between *r2d2* and *loqs* mutant situation are indicated by an arrow (pointing from *r2d2* to *loqs* mutant).

Supplementary Figure 3: Further binding studies using single dsRBDs and alternative substrates

A) Binding curves corresponding to the Kds given in figure 1B of the main manuscript. The RNA sequences and structures are indicated above and color-coded according to the titration curves.
B) Binding curves recorded using fluorescence anisotropy for individual Loqs-dsRBD1 (left panel) and dsRBD2 (right panel). The experiments are analogous to those shown in Fig. 1b of the main text.
C) Direct comparison of the binding curves obtained with EMSA and fluorescence anisotropy. The shape of the curves is comparable.
D) To verify the absence of sequence-specific effects, we tested binding of full-length Loqs-PD to miR-8 derived model substrates (right panel); the left panel compares the obtained K_D values between the miB-8 and bantam derived substrates.

Supplementary Figure 4: The two Loqs-PD dsRBDs show canonical fold and RNA binding mode

A) The $^{1}H,^{15}N$-HSQC spectra of the single domains (colored) overlay nicely with the tandem Loqs-$PD_{\Delta NC}$ spectrum. Additional black peaks can be assigned to the linker, which basically uncouples the two domains.
B) The correlation time plotted against the residue number for the individual domains (light colored) and the tandem construct (dark) confirms the independence of both domains due to the flexible long linker. **C)** 10 lowest energy Rosetta structures of dsRBD1 (blue) and dsRBD2 (cyan) of Loqs. **D)** DALI alignment of

dsRBD1 and dsRBD2 with the respective top hits. The models suggest both domains bind RNA via the conserved dsRBD binding mode.

Supplementary Figure 5: Site-specific cross linking of individual Loqs dsRBDs and binding studies with the nicked siRNA

A) Overview of the siRNA substrates employed in the cross-linking studies. The reactive thio-Uridine is indicated in red.
B) Results of the cross-linking studies obtained with the individual Loqs-dsRBDs. A representative gel image is shown on the top, the quantification of 3 independent experiments is shown below (average ± SD).
C) Binding studies using the nicked siRNA. The model substrates used are shown on the top left, an asterisk indicates the fluorescently labeled uridine residue. Both EMSA-measurements as well as fluorescence anisotropy measurements demonstrate comparable binding of the intact and the nicked siRNA. This is true for both Loqs-PD$_{\Delta NC}$ and for the individual dsRBD2 (bottom right).

Supplementary Figure 6: Observed intermolecular PRE for a TEMPO spin label attached to both ends

A) Results of the cross-linking studies obtained with the RNA duplexes mimicking the miRNA/miRNA* duplex. The respective structures are presented with the cross-linked thio-uridine indicated in bold (always in the red strand). Despite the presence of an internal bulge (e.g. for miR pos. 9 thio-uridine), we observed preferential cross-linking at the ends of the RNA duplex. The PRE calculated as I_{para}/I_{dia} is plotted against the residue number. The two domains are colored in blue and green respectively. The top diagram shows data for the spin label at the more stable end while the bottom one shows the results for the less stable end. For both cases weak PRE effects can be observed. However, for the stable end labeling more and stronger PREs are observed.
B) PRE experiment using a different RNA, where base pairs in the terminal region of the duplex were altered (grey boxes in A and B) to invert the thermodynamic stability and create a much increased thermodynamic assymetric of the RNA duplex.

Supplementary Figure 7: Characterization of Loqs-PD linker deletion mutants

A) Amino acid sequences of wildtype Loqs-PD and linker mutants are shown.
B) CSPs for the four linker mutants compared to the wildtype are shown. Overall, shortening the linker leads to low CSPs. **C)** CSPs for linker mutant RNA titrations are plotted. The same RNA as in figure 5B of the main manuscript was used. The binding mode is gradually affected by the linker length. However, overall line broadening increases with shorter linker leading to a loss of detectable signals (negative bars). This could be due to sliding or higher order complexes. **D)** P(r) SAXS curves of the wildtype protein and two linker mutants confirm the more compact state of the protein comprising a shorter linker.
E) The linker mutants in complex with RNA yield shorter maximum distances than the wildtype. **F)** Binding studies with Loqs-PD$_{\Delta NC\Delta 41}$ demonstrate that RNA binding is still possible at the concentrations employed for the fluorescence anisotropy assay. The binding affinities measured are indicated.
G) The interaction between the longest deletion mutant (Loqs-PD$_{\Delta 41}$) and Dcr-2 remains intact as demonstrated by successful co-immunoprecipitation. In this case, we used a genome-engineered cell line that carries a double FLAG-tag at the C-terminus of Dcr-2. We used this for immunoprecipitation and could show that an N-terminally myc-tagged, transiently transfected Loqs-PD full length as well as the linker deletion mutant co-immunoprecipitates with Dcr-2. Analogously tagged and transfected Renilla-luciferase or GFP, however, do not co-immunoprecipitate with Dcr-2, demonstrating specificity.

Supplementary Figure 1

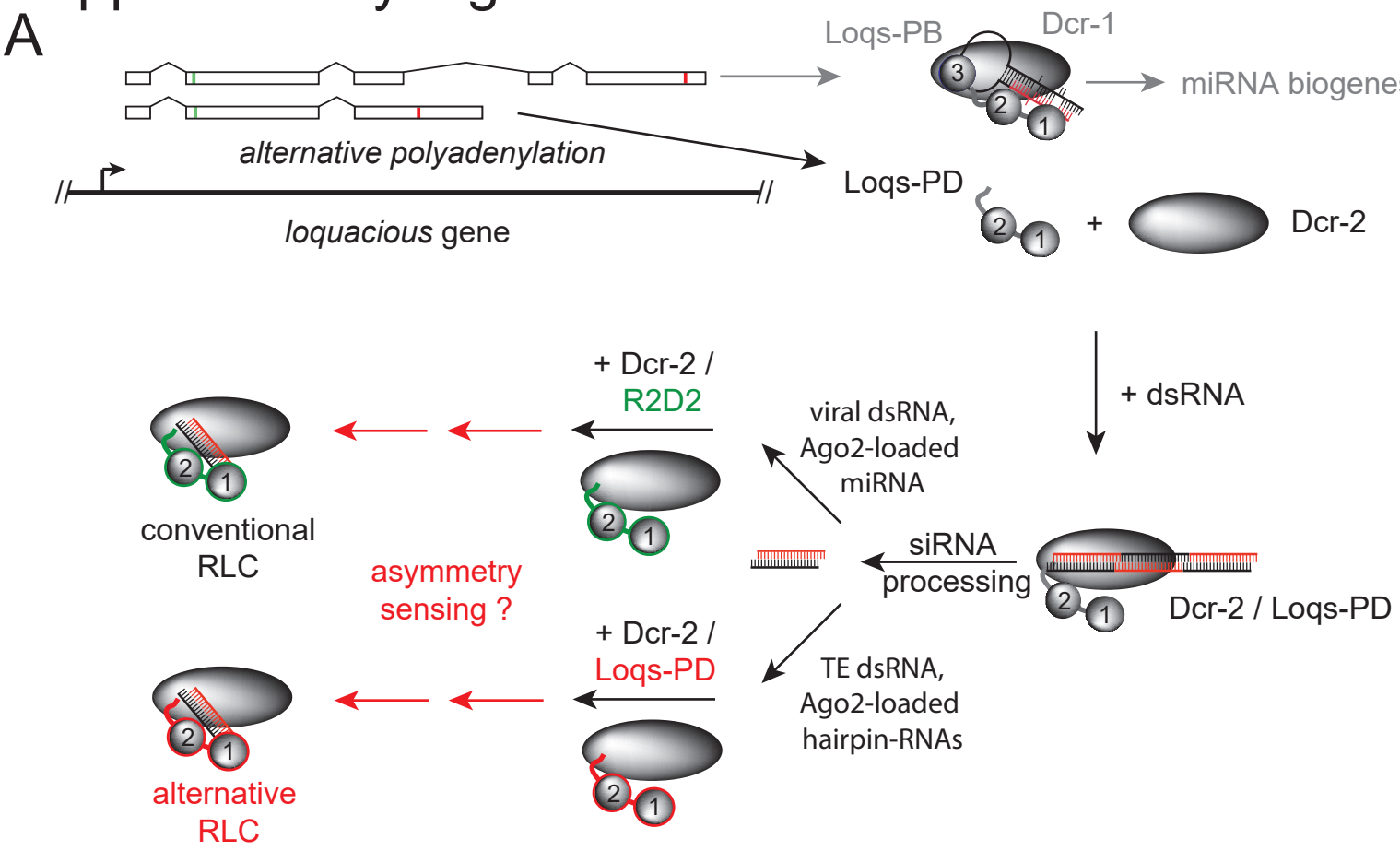

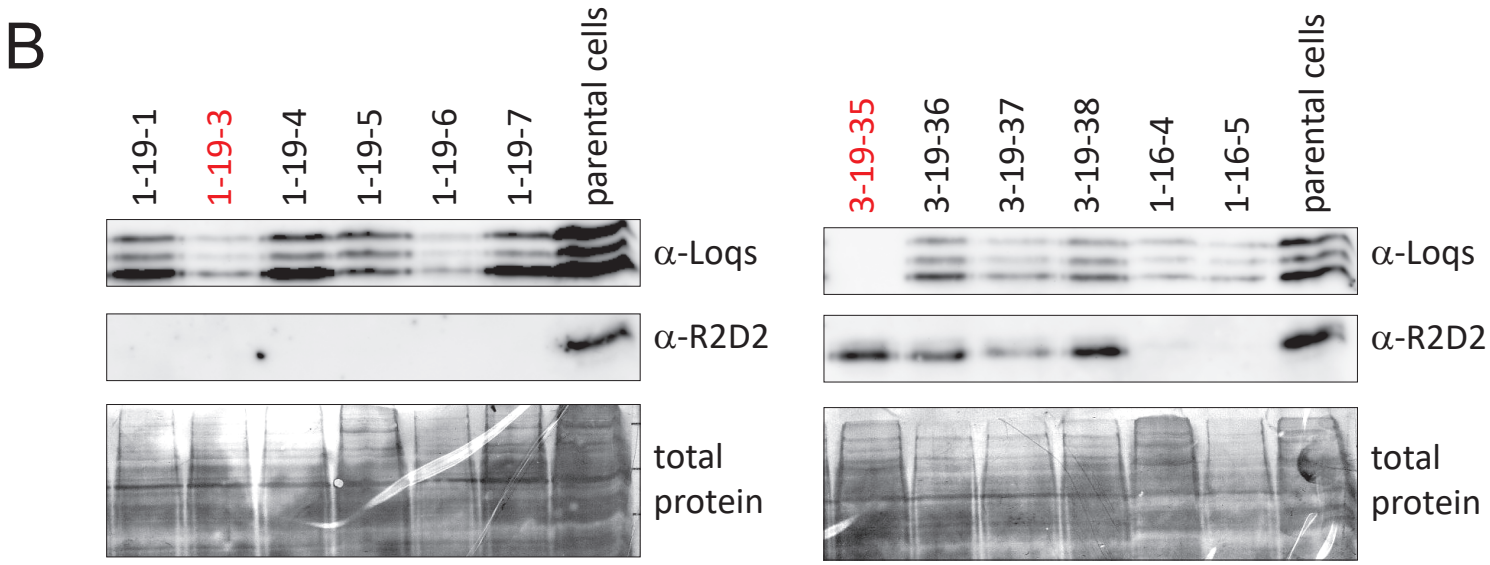

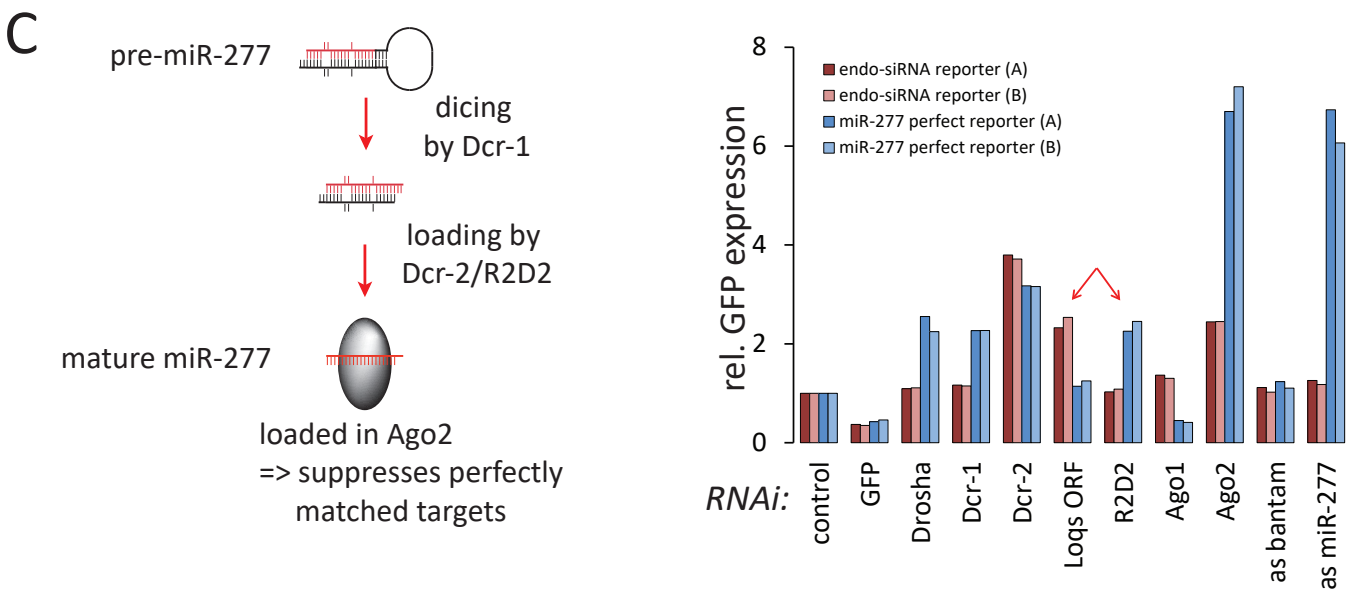

Supplementary Figure 2

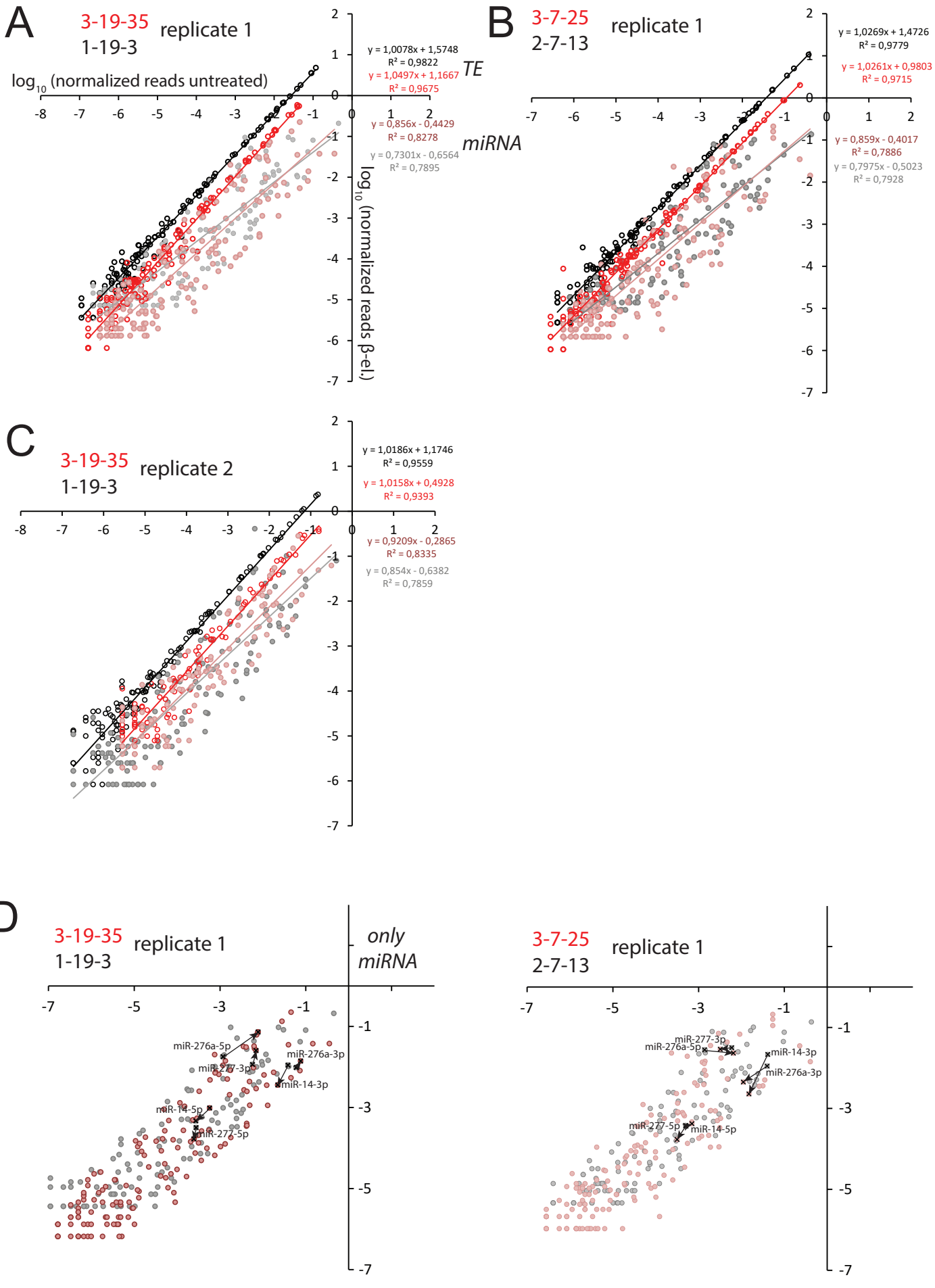

Supplementary Figure 3

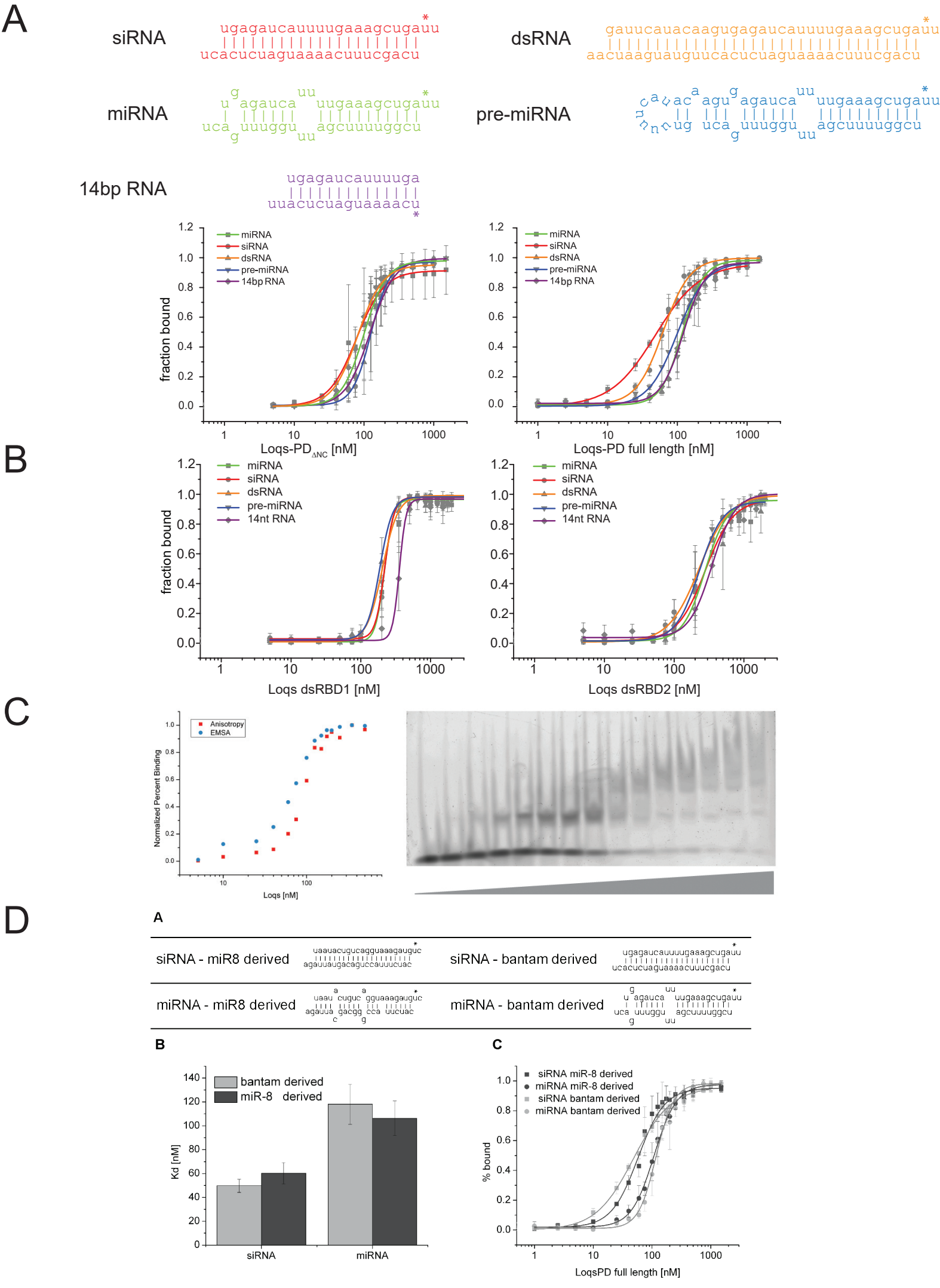

Supplementary Figure 4

A

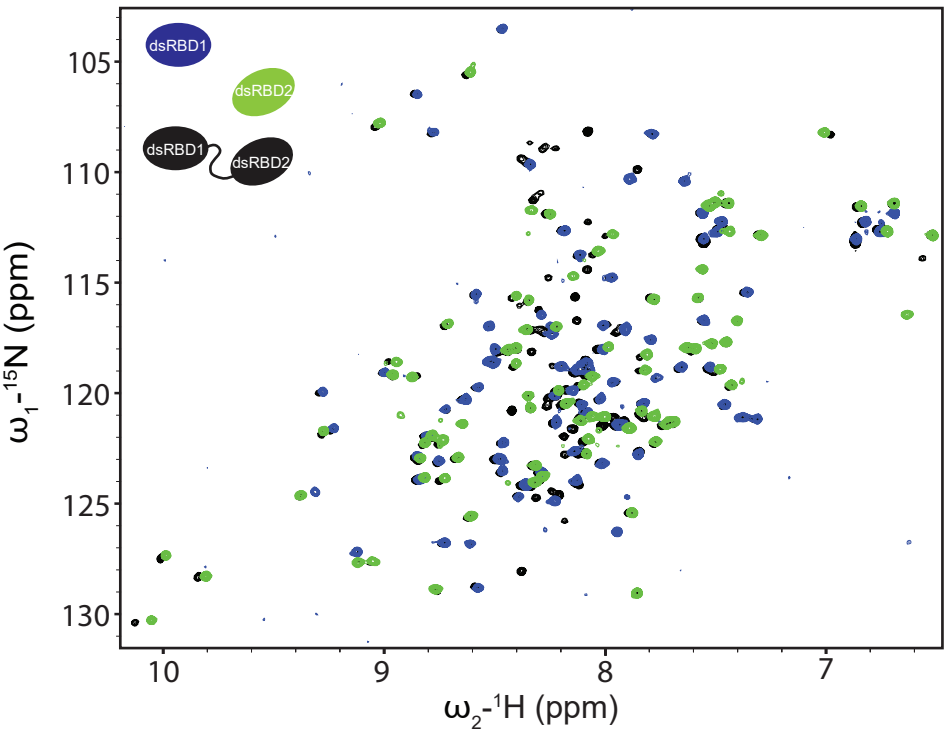

B

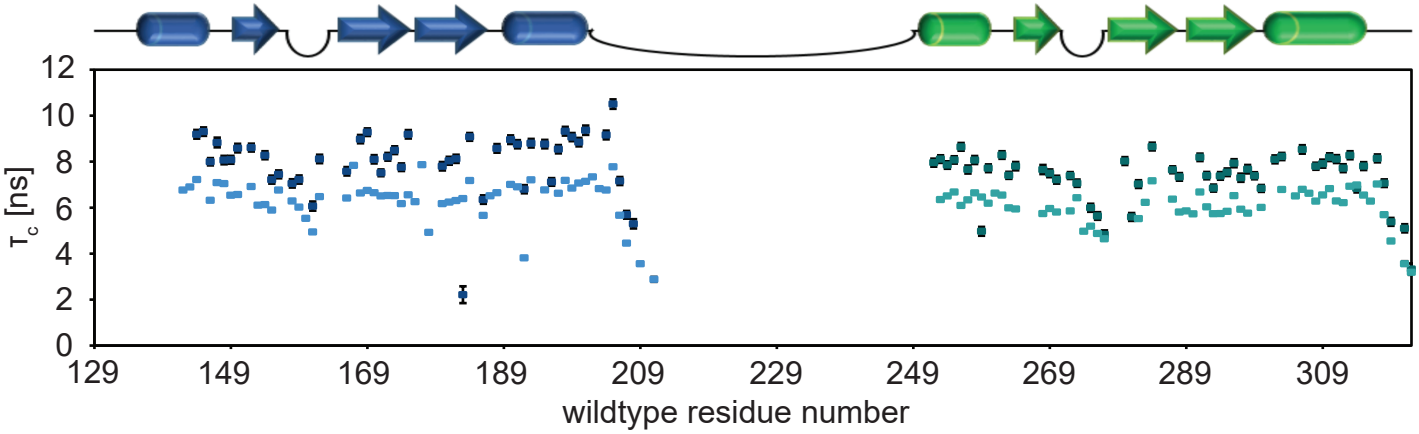

C

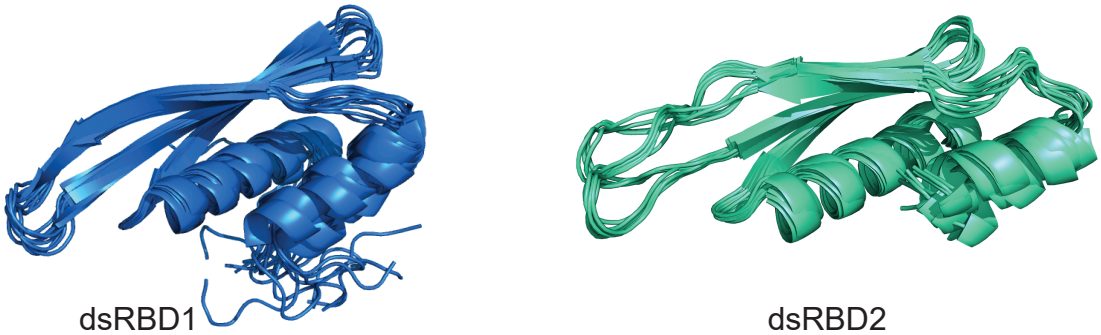

D

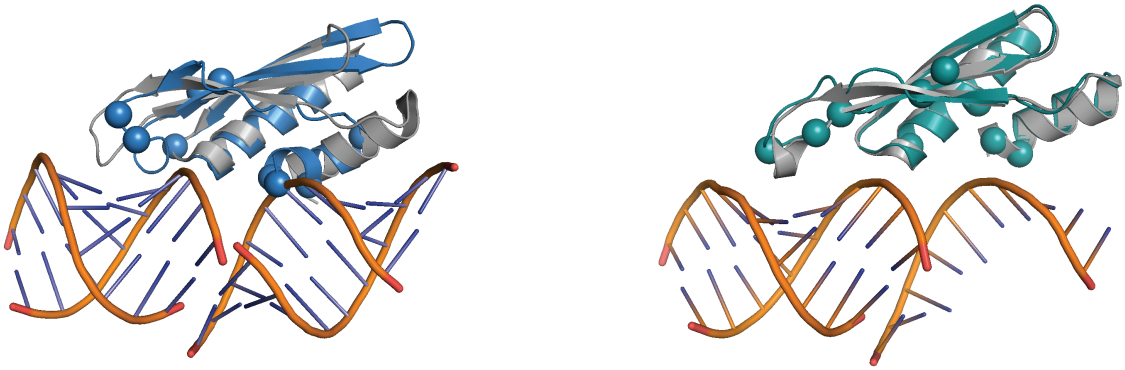

Supplementary Figure 5

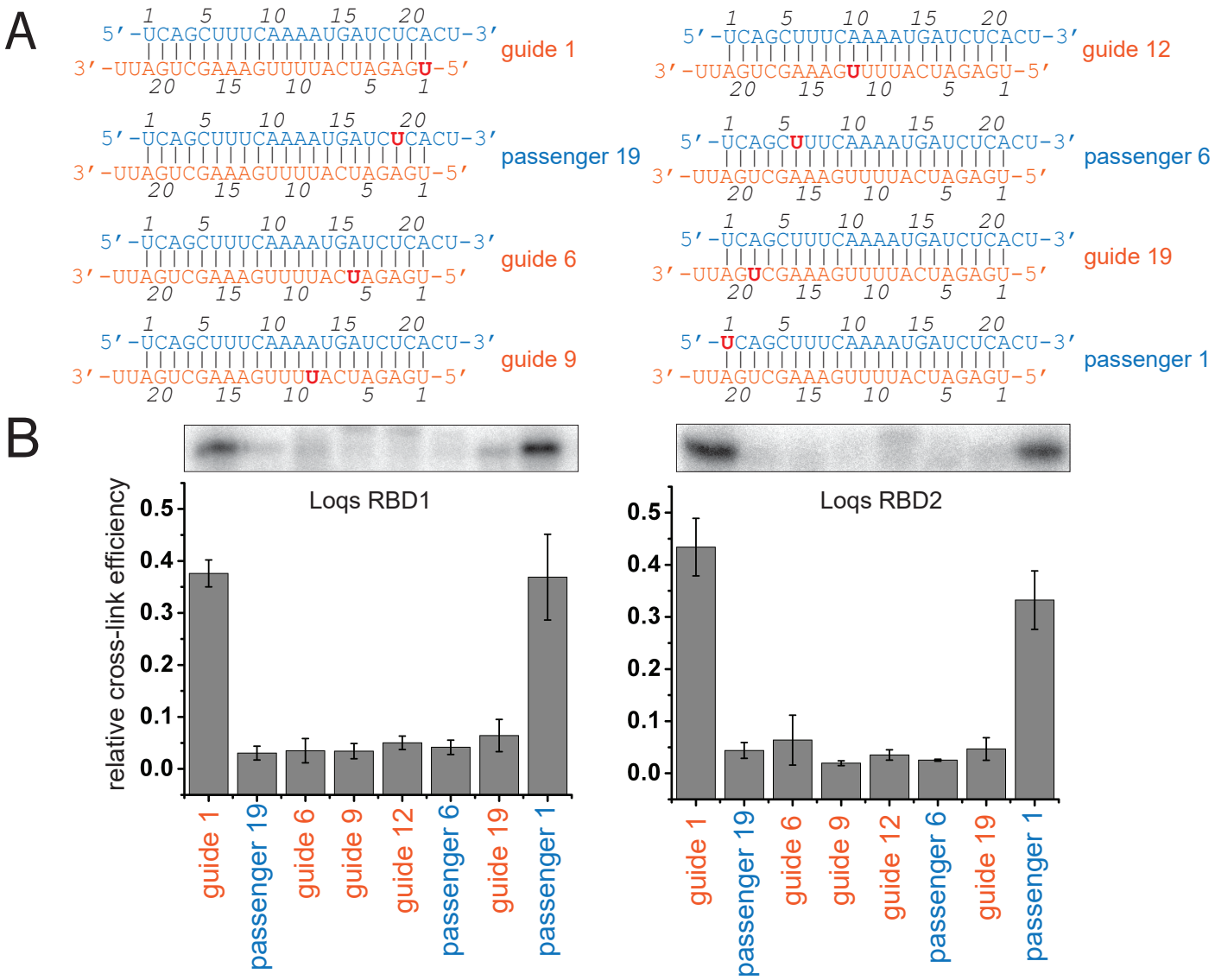

Supplementary Figure 6

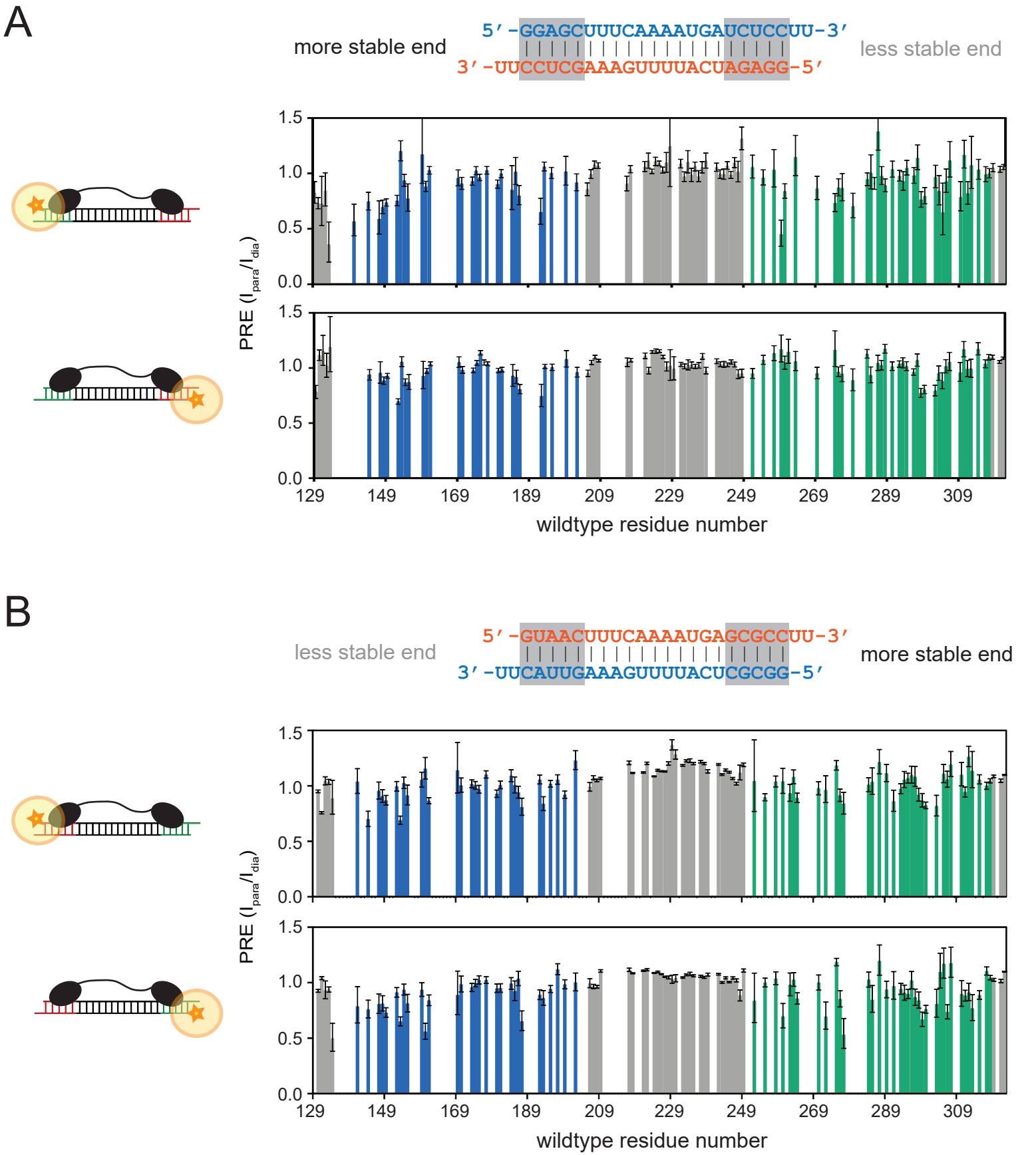

Supplementary Figure 7